Strengthening Due to Interlamellar Constraint in Oriented Syndiotactic Styrene–*p*-Methyl Styrene Copolymer

D. Pricope, D. M. Shinozaki

Department of Mechanical and Materials Engineering, The University of Western Ontario, London, Ontario, Canada N6A 5B9

Received 27 November 2001; accepted 25 February 2002

ABSTRACT: Channel die compression has been used to form highly oriented syndiotactic styrene–*p*-methylstyrene copolymer in the solid state. The highest forming temperatures were at or near the nominal unoriented melting point (247°C). The oriented materials produced at 245 and 220°C were examined by differential scanning calorimetry, wide-angle X-ray diffraction, and dynamic mechanical thermal analysis. The measured increases in modulus, which resulted from the forming of the copolymer could be related to the microstructural changes in the material. The analysis of mechanical properties with a simple Takayanagi model showed that the high modulus above the glass transition temperature in oriented samples was at least partly due to an interlamellar constraint of the kind suggested by Arridge and co-workers. The magnitudes of the constraint factor that were estimated in the modeling process were consistent with the observed microstructural changes. © 2002 Wiley Periodicals, Inc. J Appl Polym Sci 86: 2312–2321, 2002

Key words: syndiotactic; styrene *p*-methylstyrene; orientation; modulus; modeling; lamellar constraint; amorphous

INTRODUCTION

Syndiotactic styrene *p*-methyl styrene copolymer (SPMS) has been the subject of recent interest.[1] Much of the literature on this material has dealt with the crystallization behavior of its close analogs: syndiotactic polystyrene (sPS) and syndiotactic poly(*p*-methyl styrene (s-PPMS). Both can exist in a variety of different crystal structures, mesomorphic and clathrate forms.[2–7]

The development of orientation with tensile drawing has been examined in both sPS,[8–11] and to a lesser extent in s-PPMS.[12] In the study of drawing of SPMS, the maximum draw ratio obtainable before tensile fracture intervened was 4.3[1]. The crystalline melting temperature and the lamellar dimensions increased with increasing draw temperature. It was of interest to extend the experiments to larger plastic strains in an attempt to improve the degree of orientation and mechanical properties in the chain axis direction.

From the practical viewpoint, it is useful if the increase in modulus that is produced by the development of orientation is stable at high temperatures. This implies that for an oriented crystalline polymer, the microstructure, which consists of oriented lamellae, should be stable. Large strain solid-state extrusion has been used to fabricate microstructurally stable, high modulus material, notably in polyethylene.[13] An important practical aspect of the extrusion process is the suppression of cavitation during plastic deformation as a consequence of the high hydrostatic pressures that develop during forming. Plane strain channel die forming can also produce hydrostatic pressures and allow large plastic strains to develop without fracture. This potential to develop much higher stable strains and, hence, much more highly oriented material during forming was a major motivation to use this method in the present experiments. Such forming processes have been applied to nylon[14] and recently to polypropylene.[15]

An important part of the evaluation of the success of the forming process is to understand the relationship between the microstructure and the mechanical properties. A study of the dynamic mechanical properties of unoriented sPS has shown that there was a significant microstructural constraint effect that has been shown to affect the modulus of the material at temperatures above the glass transition.[16] The present work examines this phenomenon in highly oriented, channel-die-formed SPMS.

EXPERIMENTAL

Pellets of SPMS (Questra MA406) were obtained from Dow Chemical. The molecular weight characterization of the material showed that $M_w = 2.94 \times 10^5$ and $M_n/M_w = 2.80$. X-ray diffraction patterns and thermal properties were analyzed to show that the copolymer consisted of ~7% *p*-methylstyrene. The SPMS was

Correspondence to: D. M. Shinozaki.

Journal of Applied Polymer Science, Vol. 86, 2312–2321 (2002)

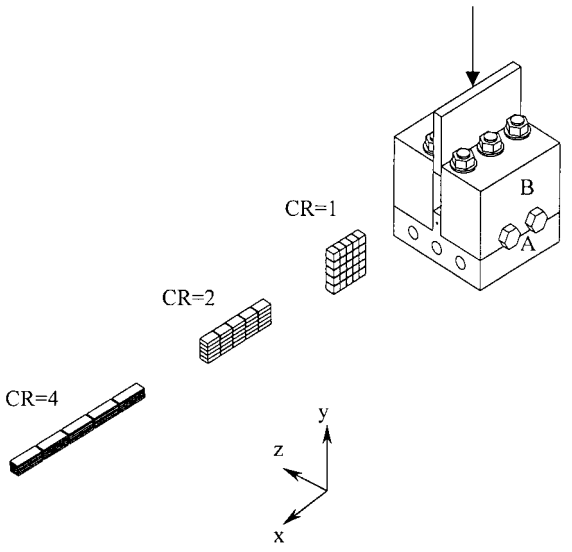

Figure 1 Schematic diagram of the channel die forming process. The orientation direction is parallel to x.

slowly melt extruded into cylindrical samples with a diameter of 60 mm. Rectangular samples (20 × 20 × 5 mm) were cut from the central portion of the extruded rod, which was slowly cooled from the melt. This initial material was isotropic. The surfaces of the sample were polished to a smooth finish by standard metallographic techniques. For low temperature forming, the surfaces were lubricated with silicone oil to reduce friction at the walls. A grid with an element size of 4 × 4 mm was marked on the side surfaces to monitor deformation during the forming operation.

The die was constructed in two parts (Figure 1). Cartridge heating elements were inserted into the bottom plate (A), which was brass for high thermal conductivity. The side walls (B) were steel. The temperature was controlled to within ±1°C. The sample was preheated for ~30 min, then compressed in the die at the predetermined rate. The forming experiments were run over a wide range of temperatures ($20 < T < 249$°C). Of particular interest were the forming experiments at the melting peak of SPMS (247°C). The compression rate varied from 0.1 to 20 mm/min, with most experiments run at 3 mm/min. The amount of deformation was characterized by the compression ratio (CR), which was the ratio initial height/final height of grid elements marked on the specimen. For inhomogeneously deformed samples, the CR was measured locally for one element of the grid, and subsequent characterization and testing was performed on samples cut from the selected grid element. This procedure was carefully followed for the thermal analysis and dynamic mechanical testing so the CR reflected as closely as possible the true local value of amount of deformation.

Thermal properties were measured with a Perkin Elmer DSC7 differential scanning calorimeter (DSC), run normally at a scanning rate of 10°C/min. For partially crystallized samples, in which crystallization was expected during the DSC run, a fast scan rate (80°C/min) was used to minimize the amount of crystallization occurring at low temperatures during the thermal analysis of slowly crystallizing materials. This procedure followed one suggested by Krzystowczyk et al.[17] The instrument was carefully calibrated for temperature and heat flow to ensure accuracy from test to test.

The dynamic mechanical properties of the oriented material were measured with a Polymer Laboratories DMTA, which measured storage modulus and loss tangent as a function of temperature and frequency. The heating rate was 2°C/min. The measurement was made in bending mode at 1 Hz., using a cantilever beam configuration. A relatively sensitive load transducer allowed for the testing of thin samples with dimensions 6 × 10 × 0.6 mm. The long axis of the specimen was cut parallel to x in Figure 1 (the direction of orientation of the molecular axis after forming), and the bending axis in the DMTA was parallel to z. Thus, the tensile modulus parallel to the orientation direction was measured.

The orientation of the crystalline phase was examined using wide-angle X-ray patterns (WAXP) exposed in transmission Laue geometry with Cu K_α radiation. The beam was parallel to the y axis in Figure 1.

RESULTS AND DISCUSSION

The progress of the forming is shown in Figure 2, in which the deformation in the xy plane of the specimen is shown. The largest strain was found in a layer just above the bottom surface. A thin slice of material parallel to the xz plane was cut carefully from this

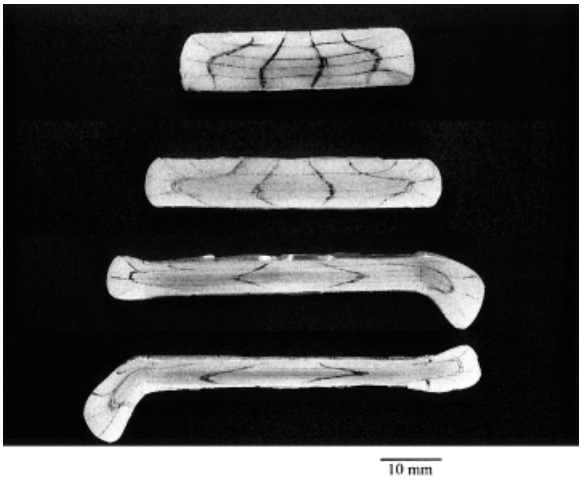

Figure 2 Photographs of the progressive deformation in forming at 220°C. The CRs are, from top to bottom, 2, 3, 5.25, and 6.

layer of maximum tensile strain for the subsequent tests.

X-ray diffraction patterns taken before and after forming are shown in Figure 3 for the two forming cases that produced the largest deformation ratios: 220°C at CR = 7 and 245°C (within the melting peak) at CR = 8. The observed diffraction maxima were

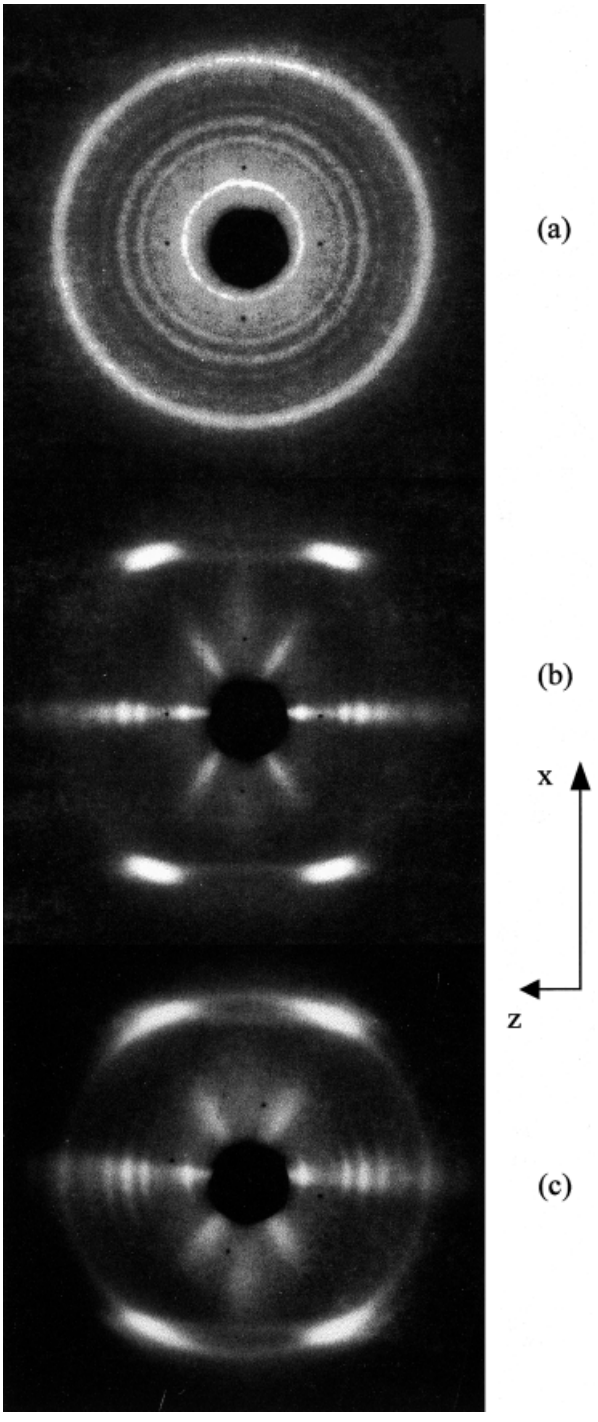

Figure 3 Wide-angle X-ray diffraction patterns taken in transmission Laue mode: (a) unoriented; (b) formed at 220°C with CR = 7; (c) formed at 245°C with CR = 8. The labeled axes correspond to those in Figure 1.

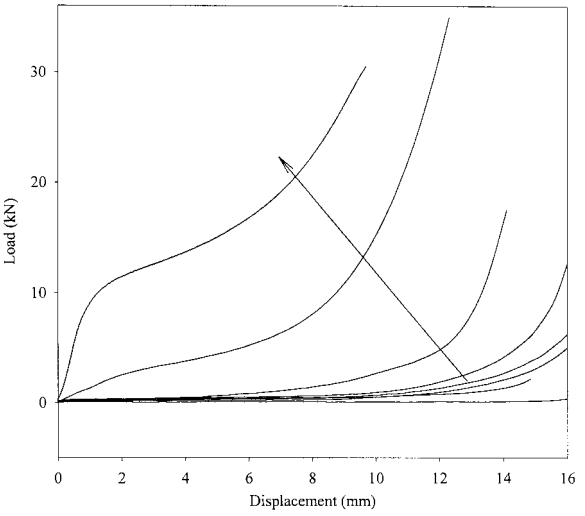

Figure 4 Load-displacement curves for channel die forming at the following different temperatures, listed in order following the direction of the arrow: 252, 249, 245, 243, 240, 220, 105, and 20°C.

consistent with earlier work on this material.[1] The outer diffraction ring (211) was concentrated into four lobes after large forming strain. The (*hk*0) and (*h*00) planes were aligned strongly with their plane normals lying in the yz plane, which is consistent with the molecular axis parallel to x, the direction of maximum tensile elongation in the formed specimen (Figure 1). It was interesting to note that the lower temperature of forming (220°C) produced better crystallographic alignment. The equatorial maxima show a smaller angular spread and the (211) lobes flatten out along layer lines in a fiber pattern.

The channel-die-forming experiments were run over a wide range of temperatures, with the expected softening at higher temperatures (Figure 4). The higher temperatures were selected around the melting peak for unoriented material as shown in Figure 5. One interpretation of the breadth of the melting peak is that the different lamellar sizes melt at varying temperatures, with the smallest lamellae melting at the lowest temperature.[18] At 252°C, the material was almost entirely liquid and compressed indefinitely at very low stresses, with no significant work hardening. At 249°C, the crystalline phase was partially melted and only a slight hardening was seen. Below 220°C, the material was completely solid, and the forming process showed a strong increase in load required at large displacement. At the highest temperatures, the lamellae were most likely isolated in a matrix of liquid, and large strain deformation involved only rearrangement in the liquid, which relaxed quickly to the unoriented state. This result is confirmed later in the observation that the modulus in the flow direction is increased by only a small amount for these higher temperatures of deformation. The two temperatures of

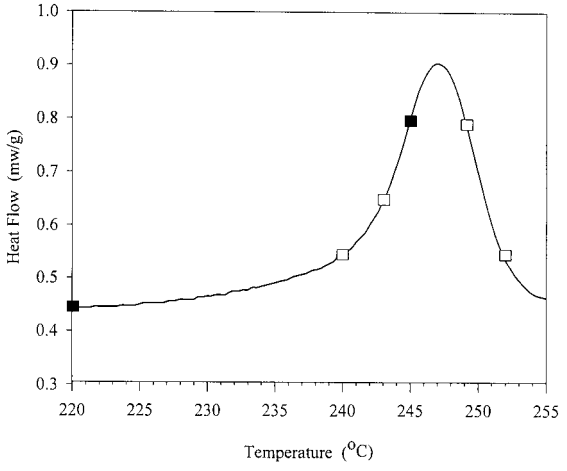

Figure 5 DSC melting peak for unoriented SPMS. The labels represent some of the forming temperatures used. The filled labels are 220 and 245°C, which are the two of most concern.

particular interest for the detailed study discussed next are 245 and 220°C, which appear in Figure 5 as filled square data points.

The thermal characteristics of the material showed striking changes after forming. The original unoriented material before forming is compared in Figure 6 with material after forming in the channel die at CR $= 7$. The curves have been arbitrarily shifted along the vertical axis, but their position along the temperature axis is correct. The differences are clearly visible. The crystalline melting peak shifted to higher temperature for forming temperatures approaching the melting temperature of the original unoriented material (245°C). In contrast, forming at the lower temperature (220°C) resulted in very little shift in the major peak. However, at the lower temperature, there was a clear double peak that developed on forming. The evolution of the double peak is shown more clearly in Figure 7. With increasing deformation, the major melting peak centered at ~247°C developed a secondary shoulder at lower temperature. The clearly distinguishable second peak was seen only at the highest CR of 7. A similar set of plots for the material formed at the higher temperature (245°C) showed only a progressive shift of the single melting peak to higher temperatures, with no multiple melting peak seen at any CR. The major peak shift for the two forming temperatures is seen in Figure 8. The melting temperatures for the secondary, low temperature peak for 220°C are not plotted here.

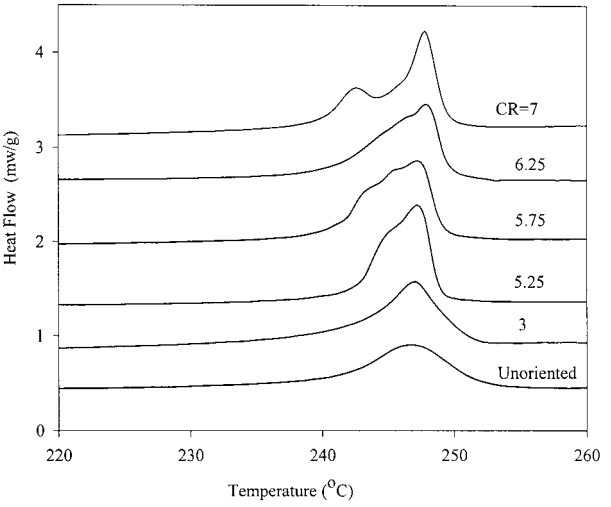

Figure 7 Changes in DSC melting peaks for samples formed to different CRs at 220°C.

The possible explanations for a multiple melting peak seen in these experiments are (1) melting and recrystallization occur dynamically during the heating scan; (2) different lamellar populations were present before the scan; and (3) different crystal structures were present.[18] Hsieh et al. have observed the appear-

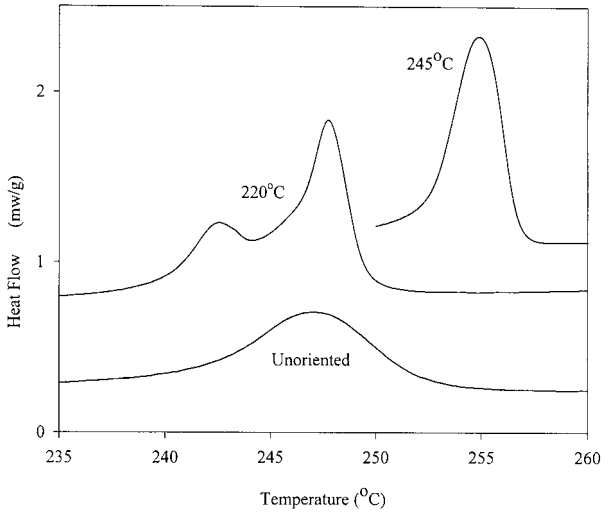

Figure 6 Comparison of DSC melting peaks for unoriented material and those formed at 220 and 245°C.

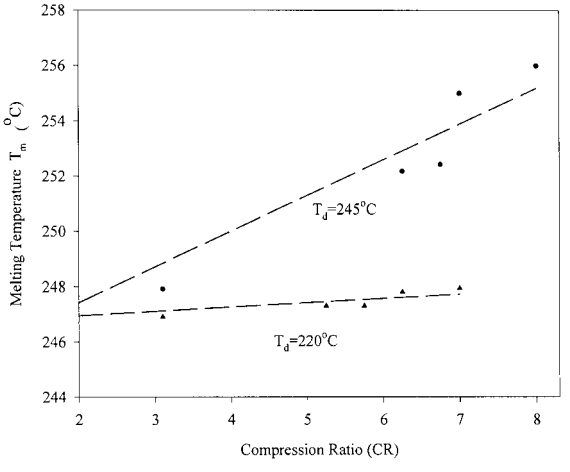

Figure 8 Comparison of the melting peak temperatures as a function of CR for the two forming temperatures.

ance of a pressure-dependent monoclinic structure in oriented ultra high molecular weight polyethylene fibers, and ascribe a double melting peak to the mixture of monoclinic and orthorhombic crystal structures.[19] A similar effect has been seen in syndiotactic polystyrene, in which the β-phase replaces the α-phase after the application of hydrostatic pressures of 118 kPa and higher.[20] The channel-die-forming process used in the present experiments involved a significant hydrostatic pressure because the deformation is constrained.

However, in earlier studies of tensile hot drawing, no double melting peak had been observed for SPMS.[1] For the present work, careful examination of equatorial X-ray diffractometer scans showed no evidence of a different crystal structure after forming at 220°C. In addition, the transmission Laue patterns of Figure 3 showed no second crystal structure after forming.

The most likely explanation for the appearance of the double melting peak was therefore the presence of different lamellar populations. Wide-angle X-ray diffraction line width measurements in earlier work on SPMS indicated that the lamellar dimensions decreased significantly with increasing tensile draw ratio.[1] The formation of a second population of smaller lamellae, generated by the large plastic strains, would have appeared as a lower temperature peak in melting. The narrowness of the discrete secondary melting peak suggested these newly formed lamellae do not have a wide distribution of sizes. It is possible that the secondary crystallization occurred in the early stages of the DSC heating run. The forming process temperature was lower than the secondary melting peak, and the secondary crystallization should appear as a dip in the DSC curve between 220 and 240°C. This was not observed in Figure 7.

The temperature increase of the melting peak with forming at 245°C in Figure 8 can be interpreted in terms of changes in lamellar thickness, as has been suggested for polyethylene.[18] The melting temperature (T_m) for polyethylene terephthalate, which is a similar to that of SPMS because polyethylene terephthalate is a slowly crystallizing material, has been shown to reflect the lamellar thickness (l) through the familiar expression:

$$T_m = T_m^\infty \left(1 - \frac{2\sigma_e}{\Delta H^o l \rho_c}\right) \quad (1)$$

where T_m^∞ is the melting temperature of an infinitely large crystal, σ_e is the surface energy of the lamellar longitudinal surface, ΔH^o is the heat of fusion of an ideal crystal, and ρ_c is the density of the crystal. The higher CRs result in larger lamellar thicknesses for 245°C.

The lack of a double peak for 245°C (Figure 5), and the shift to much higher temperatures, suggested that the lamellae readily recrystallized during forming to produce more stable, larger lamellae. This result was seen only at high forming temperatures, which lie in the melting range of the original unoriented material. The disruption of the original lamellar population became evident only at large CRs, at lower temperatures of forming (220°C), well away from the melting point (Figure 7).

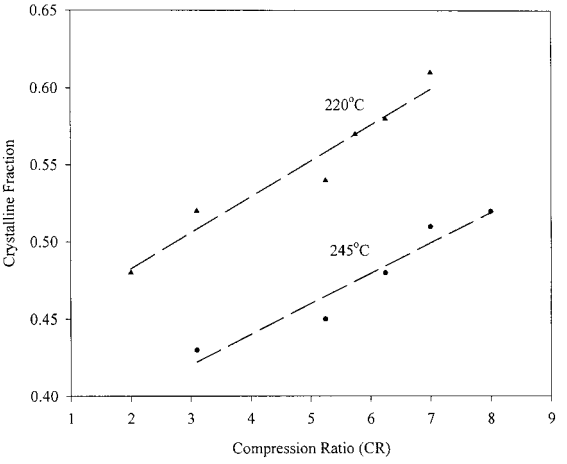

Figure 9 Amount of crystalline phase as a function of CR for the two forming temperatures.

The measurement of amount of crystalline phase (x_c) was estimated by measuring the area under the crystalline melting peak (ΔH_m) and using the known melting enthalpy ($\Delta H_o = 52.3$ J/g):[21]

$$x_c = \frac{\Delta H_m}{\Delta H_o} \quad (2)$$

The progressive increase in crystalline content with increasing CR for both forming temperatures is shown in Figure 9. The sample compressed at 220°C showed a consistently higher crystallinity than the one compressed near the melting point. The concomitant evidence that a second population of smaller lamellae appeared with forming suggested that the large plastic strains nucleated a significant number of new, small lamellae. Forming closer to the melting point resulted in the reduction in number of lamellae. This result implied the forming of larger lamellae.

The glass transition temperature also changed with deformation, as shown in Figure 10, increasing more at the lower forming temperature. This result is consistent with a strained amorphous phase in which the molecules were frozen into a nonequilibrium state, which according to some work can contribute to the heat of fusion.[22] However, this contribution was very small. A significant strained amorphous phase should also have affected the mechanical properties of the material. In the DMTA tests discussed later, the heating scan during the measurement of the dynamic me-

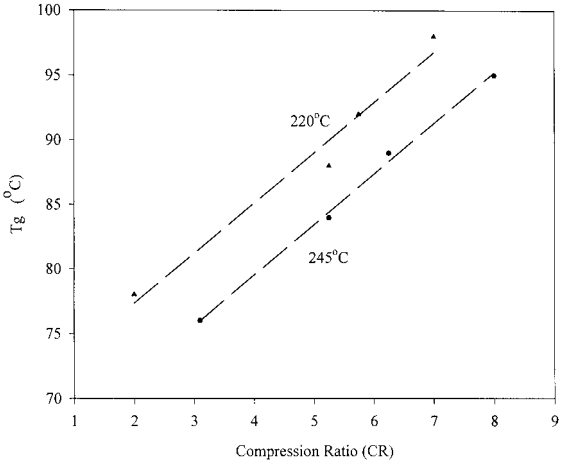

Figure 10 Glass transition temperature as a function of CR for the two forming temperatures.

chanical properties should have relaxed the amorphous phase as the test temperature increased beyond the glass transition temperature (T_g), appearing as a decrease in measured modulus. To test this idea, two successive DMTA runs were made on one specimen. No appreciable difference in modulus was found, suggesting the formed material did not contain enough highly strained amorphous material to influence the mechanical or thermal properties.

Mechanical properties

The effect of varying the compression ratio on the storage modulus is shown in Figure 11, for forming at 245°C, just below the melting point. It should be noted that the modulus was plotted on a linear scale, not

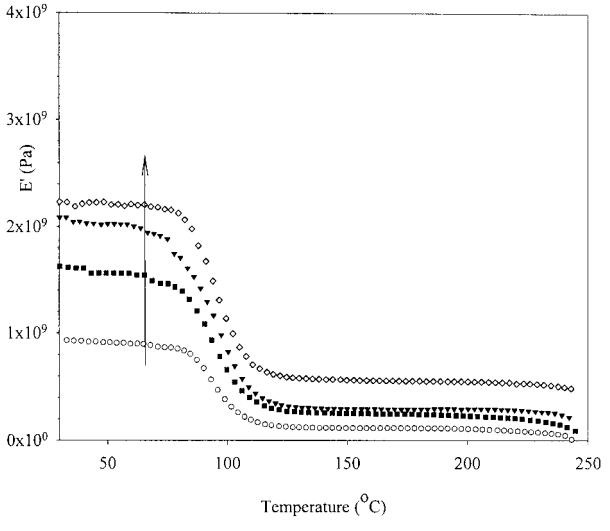

Figure 11 Temperature-dependent storage modulus as a function of CR for the forming temperature of 245°C, with CR = 1, 3, 5, 6.25, or 8 in order following the direction of the arrow. Note that CR = 1 and CR = 3 are identical, so only one is shown.

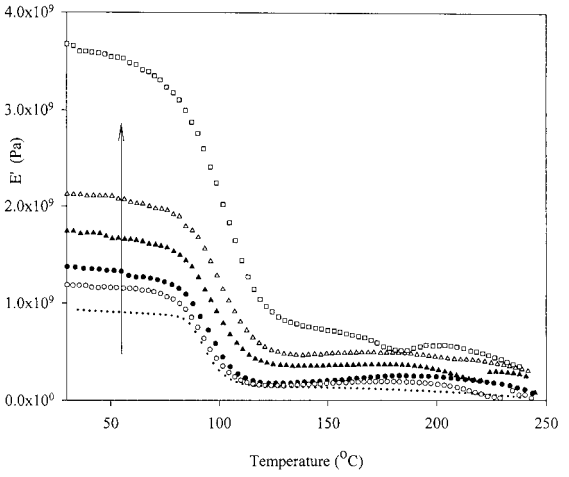

Figure 12 Temperature-dependent storage modulus as a function of CR for the forming temperature of 220°C, with CR =1, 2, 3, 5.25, 6.25, or 7, in order following the direction of the arrow.

logarithmic as is often used. The glass transition for the amorphous phase was observed below 100°C. At CR = 3, there was virtually no increase in modulus across the temperature range tested, which is consistent with the previous observation that there was negligible change in the microstructural parameters (lamellar dimensions, amount of crystallinity, or T_g). The modulus increased overall with further increases in CR.

The DMTA test involved a slow heating rate and was effectively a dynamic annealing process. Nevertheless, the lamellar microstructure appeared to be stable over the test, as no significant changes in modulus are seen with increasing DMTA test temperature. The modulus remained remarkably steady to the melting point (247°C).

Forming at the lower temperature, 220°C, the maximum modulus achieved was higher than that produced at 245°C (Figure 12). The presence of a smaller lamellar population appeared to make the microstructure thermally unstable, as the high temperature modulus decreased with increasing temperature for all CR, as would have been expected for annealing. It should be noted that the drop in modulus with increasing temperature is not a desirable property for practical applications.

At very low forming temperatures, the deformation in the channel die was limited by specimen cracking. However, even with limited CR at these temperatures, a strengthening was observed. However, the annealing occurring during the DMTA test results in an anomalous rise in modulus at the glass transition for the specimen formed at 105°C (Figure 13). This result was probably an indication of some further crystallization occurring on heating the disrupted lamellae produced by the plastic deformation of the forming

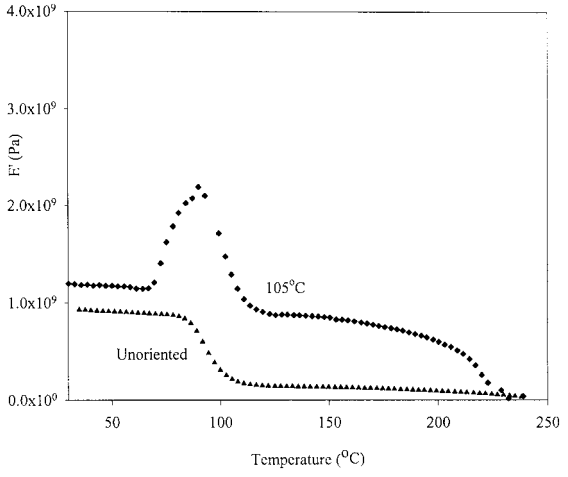

Figure 13 Temperature-dependent storage modulus for forming at low temperature (105°C) compared with unoriented material. CR is limited to 2.8 for this temperature.

process. At higher temperatures, the recrystallization presumably occurred dynamically during the forming process.

The forming parameter that most strongly affected the final properties was the deformation rate. The storage modulus for samples formed at 240°C and CR = 8 are shown in Figure 14 for compression rates of 0.3 and 3 mm/min. The lower forming rate resulted in a much higher modulus material. However, such slow processing speeds would make the forming process unreasonably long and impractical.

Micromechanical modeling

Insight into microstructural effects in orientation strengthening can be obtained by fitting micromechanical models to the measured properties. The Voigt

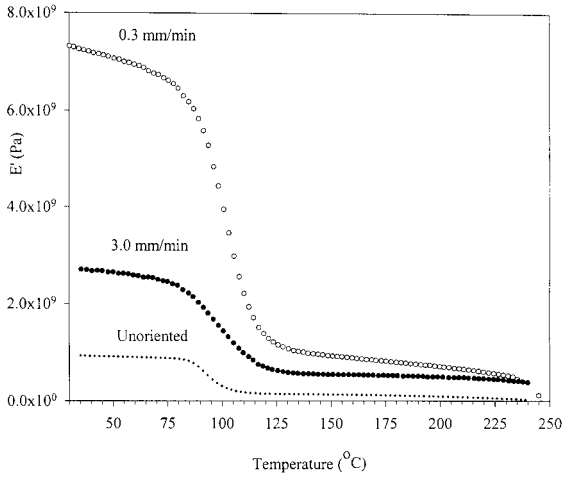

Figure 14 Effect of forming rate on storage modulus. The forming temperature is 240°C and CR = 8 for the two top curves.

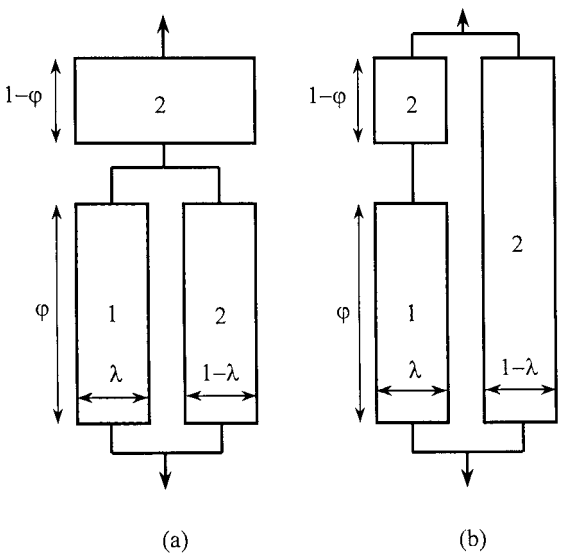

Figure 15 Schematic diagram of two Takayanagi models. The parameters are defined in the text.

and Reuss models define simple upper and lower bounds to the average properties of this two-phase composite material consisting of crystalline and amorphous phases:

$$E_{co} = (1 - x_c)E_a + x_cE_c \tag{3}$$

$$\frac{1}{E_{co}} = \frac{(1 - x_c)}{E_a} + \frac{x_c}{E_c} \tag{4}$$

where E_{CO} is the composite modulus, x_c is the amount of crystalline phase, and E_c and E_a are the moduli of the crystalline and amorphous phases, respectively. Takayanagi introduced a variation of these two phase models by dividing one of the phases into two components and adding it to either the Voigt model in series or to the Reuss model in parallel.[23,24] These are represented by eqs. 5 and 6, respectively:

$$\frac{1}{E_{co}} = \frac{\varphi}{\lambda E_1 + (1 - \lambda)E_2} + \frac{1 - \varphi}{E_2} \tag{5}$$

$$E_{co} = \lambda\left(\frac{\varphi}{E_1} + \frac{1 - \varphi}{E_2}\right)^{-1} + (1 - \lambda)E_2 \tag{6}$$

where E_1 and E_2 are the moduli of the dispersed and contiguous phases, respectively, and λ and φ are parameters that are related to the phase proportions and mixing state of the phases, respectively. The product $\varphi\lambda = x_1$ is the volume fraction of the dispersed phase (Figure 15). There are two possible cases: for a dispersed crystalline phase, $\varphi\lambda = x_c$, and for a dispersed amorphous phase, $\varphi\lambda = x_a$.

Each of the two possible cases has been applied in earlier work.[16,24,25] The model is useful in assigning

some parameters that are qualitatively related to the microstructure of the formed material, although it is not possible to determine the exact relationship between microstructure and model. In the region directly over the glass transition, the loss factor (tan δ) is large, and Gray and McCrum suggest that simple composite models like the one proposed by Takayanagi are inaccurate if only the real part of the complex modulus is used.[26] Outside the transition region, the storage modulus can be used accurately: firstly, for $T < T_g$, where the two phases are hard and elastic, and secondly, for $T < T_g$ where the amorphous phase becomes rubbery. This procedure is followed here.

For a blended polyvinyl chloride/nitrile butadiene, Ward has suggested the model (a) in Figure 15 provided the closest fit to the experimental data for unoriented material.[25] Takayanagi used the same model to characterize oriented semicrystalline polymers.[24] Earlier, St. Lawrence et al. applied the Takayanagi model to unoriented syndiotactic polystyrene[16] and concluded that model (b) was most appropriate. In the present experiments, both models were initially considered as possible.

The crystallinity and composite modulus were measured as a function of temperature (the amount of crystalline phase increased slightly with T resulting from the dynamic annealing that occurred during the DMTA test). Because the material was oriented and because the crystal structure was similar, the c-axis modulus of $E_c = 84.5$ GPa was used for the modeling. The amorphous phase modulus was measured under DMTA test conditions identical to the SPMS tests, using atactic polystyrene, over the entire temperature range of interest (35°C $< T <$ 250°C).

Initially, for each of the two Takayanagi models in Figure 15, the contiguous phase 2 could be either crystalline or amorphous. The model parameters that fitted the experiment most closely for $T < T_g$ were calculated, resulting in a number of feasible combinations. These various possible models were then used to calculate a modulus for $T > T_g$ where the amorphous phase was rubbery.

After considering the various physical aspects of the problem, the model that appeared to agree best with the experimental results over the entire temperature range was the parallel-series model with the amorphous phase contiguous. This model is labeled model (b) in Figure 15, with phase 1 as crystalline and phase 2 as amorphous.

Curve A in Figure 16 shows a typical result of fitting this Takayanagi model for $T < T_g$, then extrapolating its predicted modulus to the higher temperature region $T > T_g$. The modulus predicted by the model at high temperatures was much lower than the experimental results. A plausible explanation for this discrepancy was found in Arridge's constraint model for

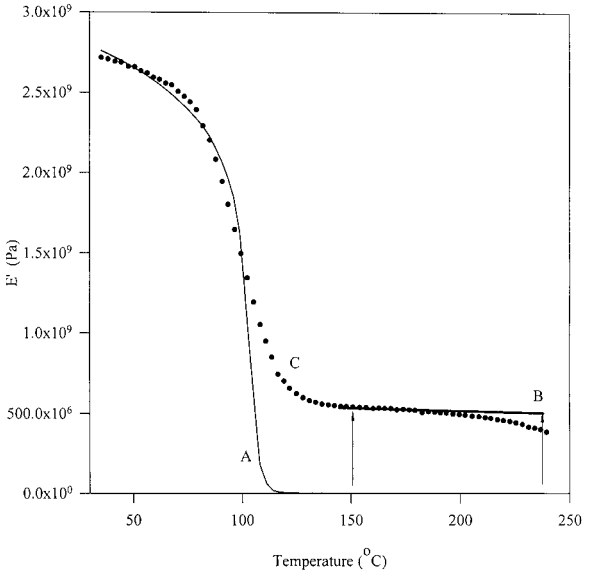

Figure 16 Example of the fitted Takayanagi model (from Figure 15 b) with a contiguous amorphous phase (2). Curve A is fitted for $T < T_g$ and extrapolated to $T > T_g$ ($\varphi = 0.865$). Curve B is corrected with a constraint factor of $K = 220$ for $T > T_g$. Curve C is the experimental modulus for a forming temperature of 240°C, with CR = 8.

lamellar polymer microstructures[27,28] as applied to unoriented syndiotactic polystyrene.[16]

Lamellar constraint

For $T > T_g$, the amorphous phase is rubbery, with a Poisson's ratio of 0.5, whereas the lamellae are much stiffer. In an oriented material, the lamellae are aligned with their plane normals parallel to the orientation direction. In uniaxial loading in this direction, the stiff lamellae constrain the much softer amorphous phase in a manner similar to rubber sheets glued between steel plates, and the experimental composite modulus is much higher than that predicted from the unconstrained phase properties. The rubbery amorphous phase is effectively stiffened by the constraint. The degree of constraint increases with increasing aspect ratio (width to thickness) of the rubbery phase, and can be quantified by a constraint factor (K) which Arridge has calculated as:[28]

$$3K = 3.52 + 0.984\left(\frac{b}{a}\right)^2 \tag{7}$$

This constraint was similar to that calculated by Gent and Lindley for a macroscopic rubber sheet bonded to steel plates:[29]

$$3K = 4 + \left(\frac{b}{a}\right)^2 \tag{8}$$

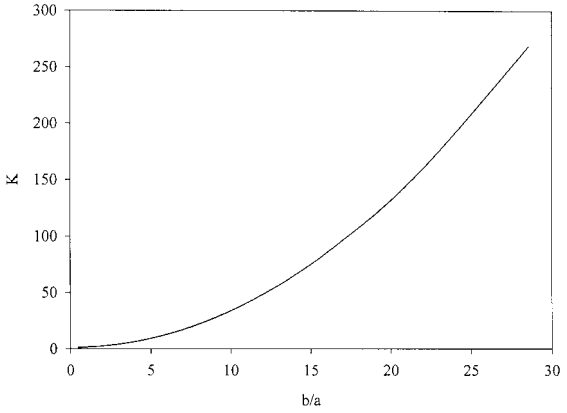

Figure 17 The Arridge constraint factor as a function of the aspect ratio of the rubbery amorphous phase.

where (b/a) is the width-to-thickness ratio of the amorphous (interlamellar phase). The use of a constraint factor to modify the effective amorphous modulus for $T > T_g$ is shown as the curve B in Figure 16, where $K = 220$. The constraint factor increases very rapidly only for large (b/a), as shown in Figure 17. Transmission electron microscopy has shown that interlamellar thicknesses were in the nanometer range, while the widths of the constrained amorphous layers were at least 5–10 μm for sPS.[16] The constraint model predictions were therefore reasonable for typical lamellar microstructures.

The micromechanical model that includes an interlamellar constraint was fitted to the DMTA results for specimens prepared under the different forming conditions, and yielded results consistent with the other experimental observations. The two forming temperatures of particular interest here (220 and 245°C) were so examined. The model parameters that were related to the microstructure (x_c, φ, λ, and K) were calculated as shown in Tables I and II.

The crystallinity consistently increased with CR for both temperatures, but reached a significantly higher value for 220°C at high CR. The parallel component of amorphous material, $(1 - \lambda)$ in Figure 15b, did not contribute to the overall strengthening of the composite because at $T > T_g$, the phase was rubbery with almost zero stiffness. The important microstructural parameter was φ, the crystalline component, which increased with CR for both temperatures. It was higher at 220°C for CR > 6 (approximately). The moduli measured for the two forming temperatures reflected these differences, confirming the validity of the model.

TABLE I
Takayanagi Parameters[a]

CR	x_c	φ	λ	K
7	0.6	0.891	0.673	195
6.25	0.58	0.864	0.671	208
5.75	0.57	0.786	0.725	237
5.25	0.54	0.728	0.741	219
3.1	0.52	0.61	0.852	156
2	0.48	0.53	0.905	152

[a] Fitted to experimental data for material formed at 220°C, with CR = 7. The Arridge constraint factor (K) is included.

TABLE II
Takayanagi Parameters[a]

CR	x_c	φ	λ	K
5	0.45	0.74	0.61	185
6.25	0.48	0.79	0.61	180
8	0.52	0.82	0.64	280

[a] Fitted to the experimental data for material formed at 245°C with CR = 8. The Arridge constraint factor (K) is included.

The drop in K with increasing CR at 220°C was related to the observation of the development of the double melting peak in Figure 6 at higher CR. This result was consistent with the development of a population of smaller lamellae suggested earlier, with presumably smaller average widths. Forming at 245°C resulted in larger lamellae, possibly thicker, with thinner interlamellar regions (as suggested by annealing observations in polyethylene with higher K and in agreement with the increase in melting peak temperature at CR = 8; Figure 8).

CONCLUSIONS

Large strain forming of SPMS using channel die compression has been used to produce highly oriented material with high crystallinity. The melting properties were measured by DSC and the mechanical properties were examined by DMTA. Comparison of forming at 220 and 245°C shows that the lower temperature produces a higher degree of orientation and higher modulus. The higher forming temperature was specifically chosen to be on the melting peak for the initial material. An analysis of the mechanical data was based on a simple Takayanagi model fitted to temperature ranges on either side of the glass transition. The fit above T_g could not be achieved without invoking an additional constraint factor suggested by Arridge. This factor involved the physical constraint of the rubbery amorphous phase by the surrounding lamellae for stresses applied normal to the lamellar plane. The constrained Takayanagi model parameters were calculated for the variously formed samples and were shown to be a physically reasonably reflection of the microstructure. The constraint of the amorphous phase by the lamellae therefore contributed significantly to the high temperature stiffening of the oriented SPMS.

This work was supported by NSERC (Natural Sciences and Engineering Research Council of Canada).

References

1. Yan, R.J.; Ajji, A.; Shinozaki, D.M. Polym Eng Sci 2001, 41, 1674.
2. Guerra, G.; Vitagliano, V.M.; De Rosa, C.; Petraccone, V.; Corradini, P. Macromolecules 1990, 23, 1539.
3. De Candia, F.; Carotenuto, M.; Guadagno, L.; Vittoria, V. J Macromol Sci Phys 1996, B35(2), 265.
4. De Rosa, C.; Guerra, G.; Petraccone, V.; Pirozzi, B. Macromolecules 1997, 30, 4147.
5. De Rosa, C.; Petraccone, V.; Guerra, G.; Manfredi, C. Polymer 1996, 37, 5247.
6. Iuliano, M.; Guerra, G.; Petraccone, V.; Corradini, P.; Pellecchia, C. New Polym Mater 1992, 3, 133.
7. De Rosa, C.; Petraccone, V.; Dal Poggetto, F.; Guerra, G.; Pirozzi, B.; Di Lorenzo, M.L.; Corradini, P. Macromolecules 1995, 28, 5507.
8. De Candia, F.; Romano, G.; Russo, R.; Vittoria, V. Colloid Polym Sci 1990, 268, 720.
9. Daniel, C.; Guadagno, L.; Vittoria, V. Macromol Symp 1997, 114, 217.
10. Yan, R.J.; Ajji, A.; Shinozaki, D.M.; Dumoulin, M.M. Polymer 2000, 41, 1077.
11. Yan, R.J.; Ajji, A.; Shinozaki, D,M, J Mater Sci 1999, 34, 2335.
12. De Rosa, C.; Petraccone, V.; Guerra, G.; Manfredi, C. Polymer 1996, 37, 5247.
13. Ciferri, A.; Ward, I.M. Ultra-High Modulus Polymers; Applied Science Publishers: London, 1977.
14. Lin, R.H.; Argon, A.S. Macromolecules 1992, 25, 4011.
15. Pluta, M.; Bartczak, Z.; Galeski, A. Polymer 2000, 41, 4011.
16. St. Lawrence, S,; Shinozaki, D.M. J Mater Sci 1998, 33, 4059.
17. Krzystowczyk, D.H.; Niu, X.; Wesson, R.D.; Collier, J.R. Polym Bull 1994, 33, 109.
18. Wunderlich, B. Thermal Analysis; Academic Press: New York, 1990.
19. Hsieh, Y.; Ju, J. J Appl Polym Sci 1994, 53, 347.
20. Sun, Z.; Morgan, R.J.; Lewis, D.N. Polymer 1992, 33, 660.
21. de Candia, F.; Filho, A.R.;Vittoria, V. Colloid Polym Sci 1991, 269, 650.
22. Meinel, G.; Peterlin, A. J Polym Sci, B 1967, 5, 613.
23. Takayanagi, M. Memoirs from the Faculty of Engineering Kyushi University 1963, 23, 41.
24. Takayanagi, M.; Imada, I.; Kajiyama, T. J Polym Sci, C 1966, 15, 263.
25. Ward, I.M. An Introduction to the Mechanical Properties of Solid Polymers; Wiley: New York, 1993.
26. Gray, R.W.; McCrum, N.G. J Polym Sci, A2 1966, 7, 1329.
27. Arridge, R.G.C. J Phys D, Appl Phys 1975, 8, 34.
28. Arridge, R.G.C.; Lock, M.W.B. J Phys D 1976, 9, 329.
29. Gent, A.N.; Lindley, P.B. Proc Inst Mech Eng 1959, 173, 111.